ELSEVIER

Contents lists available at ScienceDirect

# Materials Science & Engineering B

journal homepage: www.elsevier.com/locate/mseb





# Porous carbon foams supported rGO-ppy//rGO for asymmteric supercapacitor device

Balarabe El-yaqub <sup>a,b</sup>, Mohd Haniff Wahid <sup>a,\*</sup>, Zulkarnain Zainal <sup>a,d</sup>, Abdul Halim Abdullah <sup>a</sup>, Wan Azlina Wan Ab Karim Ghani <sup>c</sup>

- <sup>a</sup> Department of Chemistry, Faculty of Science, Universiti Putra Malaysia, 43400 Serdang, Selangor, Malaysia
- <sup>b</sup> Department of Chemistry, Faculty of Science, Nigerian Defence Academy, Kaduna State, Nigeria
- Eppartment of Chemical and Environmental Engineering, Faculty of Engineering, Universiti Putra Malaysia, 43400 Serdang, Selangor, Malaysia
- <sup>d</sup> Nanomaterials Synthesis and Characterizations Laboratory, Institute of Nanoscience and Nanotechnology, Universiti Putra Malaysia, 43400 UPM Serdang, Selangor, Malaysia

#### ARTICLE INFO

Keywords:
Compressible electrodes
Asymmetric electrodes
Binary composite
Hydrothermal
Porous carbon foams

#### ABSTRACT

Porous carbon foams (PCF) doped with binary composite of rGO-ppy was prepared using a simple dip coating method with the use of a linker and used as compressible electrodes for the asymmetric supercapacitor (ASC). Porous carbon foams were fabricated from melamine foam by carbonization in a furnace at a temperature of 300 °C and the binary composite was synthesized using hydrothermal method. The electrode materials were characterized using XRD, XPS, FTIR, BET/BJH, Raman and FESEM to confirm it's structural, functional group, surface area, thermal stability and morphological characteristics. The stress-strain tests of the samples were conducted on an electronic universal testing machine and the porous carbon foams can withstand the stresses of 14.5, 17.9 and 30.0 KPa at 40 %, 60 % and 80 % strains respectively. The mechanical properties were further examined by repeating the compression release process for 200cycles at a maintained strain of 80 %. The fabricated PCF-rGO-ppy//rGO supercapacitor device exhibited high deformation tolerance, outstanding electrochemical behaviour and enhanced cycling stability due to the flexible and compressible skeleton of the PCF and high electrical conductivity of rGO and ppy. Finally, an ASC was fabricated using PCF-rGO-ppy as cathode and rGO as the anode which showed a specific capacitance of 328.91F/g at 0.5A/g, energy density of 29.234Wh/ kg and power density of 4000 W/kg. Electrochemical impedance spectroscopy (EIS) studies showed that rGO and the porous carbon can effectively improve the charge-transfer rate from the low charge-transfer resistance (Rct) value. The fabricated electrode also showed an exceptional cycling stability of 98.89 % after 10,000 galvanostatic charge discharge (GCD) cycles.

#### 1. Introduction

Compressible supercapacitors, which can provide a stable power output under physical or mechanical deformation or compression, are becoming a key instrument in wearable electronic appliances such as smart glasses, watches, shirts, rings etc., [11,30,41]. Although the compression is a common physical and mechanical deformation faced by wearable energy storage devices, only a minimal percentage of research studies are focused on compressible supercapacitors with 3D structure[34,39,42].

The melamine sponge (MS) with a porous three-dimensional (3D) network is widely used as a compressible substrate due to its durability,

water absorption, and compressibility. For example, Niu et al. have used MS as the substrate to manufacture a compressible supercapacitor, which can maintain most of the electrochemical performances at the maximal compressive strain of 60 %. In the composition of this supercapacitor, the porous MS not only endows superior mechanical properties to supercapacitors but also provides enough space for the loading of active materials [25]. An all-solid supercapacitor is fabricated with 3D nitrogen-doped/graphene porous material as the electrode, which showed a high specific capacitance and stable electrochemical property. The as-assembled device showed a specific capacitance of 150 Fg $^{-1}$  at a current density of 0.3 Ag $^{-1}$  and a long cycle life with 85.1 % capacitance retention after 10 000 cycles at 1 Ag $^{-1}$ . In addition, the compressible

E-mail address: mw haniff@upm.edu.my (M.H. Wahid).

 $<sup>^{\</sup>ast}$  Corresponding author.

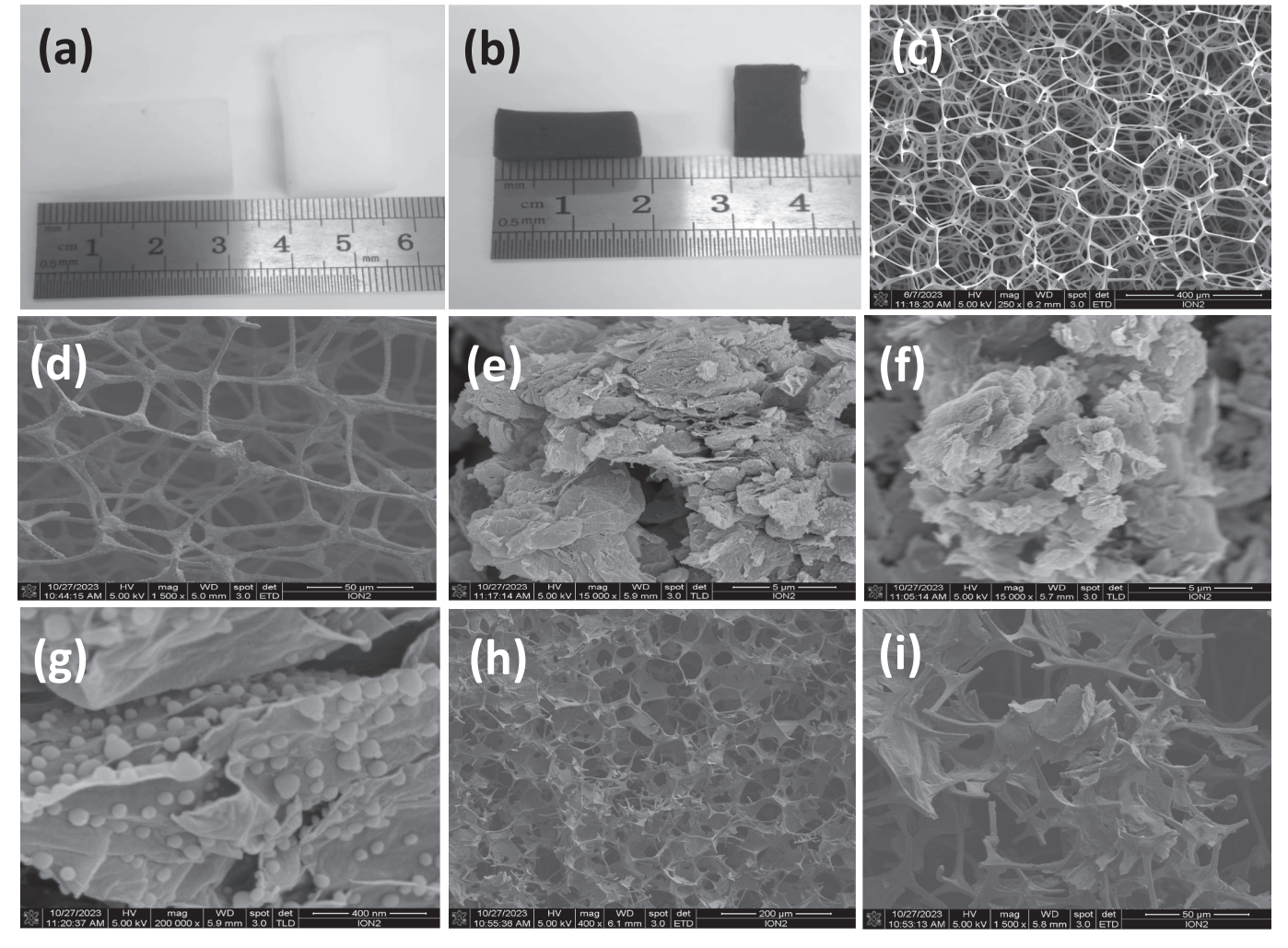


Fig. 1. Pictorial images of (a, b) MS and PCF, FESEM images of (c) MS, (d, e) PCF and (f) rGO (g) rGO-ppy and (h, i) PCF-rGO-ppy.

electrode displayed stable electrochemical performance under different compressive strains (0 %, 25 %, 50 % and 75 %) or after 100 compression/release cycles under a compressive strain of 50 % [9].

Jing et al. [11] developed monolithic electrodes for supercapacitor applications. Potassium hydroxide was used to activate the commercial melamine sponges, and used to prepare monolithic N-/O-doped carbon sponge (NOCS) electrodes. Variables such as graphitization degree, heteroatom content, and pore size distribution were regulated by adjusting the KOH/melamine sponge mass ratio. The optimal electrode demonstrated specific capacitances of  $440 \mbox{Fg}^{-1}$  at  $1.0~\mbox{mVs}^{-1}$  and  $273 \mbox{Fg}^{-1}$  at  $0.5~\mbox{Ag}^{-1}$ , and the capacitance retention remained 85.0 % after 10,000 charging - discharging cycles at  $10~\mbox{Ag}^{-1}$ .

Porous carbon foam (PCF) on the other hand can also provide these properties and even more. Because of the high content of carbon in porous carbon foams compared to melamine sponge, porous carbon foams will tend to provide more advantage towards producing a better compressible electrode.

Polypyrrole (PPy), a common conductive polymer material, has attracted tremendous attention owing to the advantages of easy synthesis, excellent specific capacitance and inherent polymer flexibility [7,36].

However, undesirable rate performance and cycling stability are inevitable flaws of PPy. Recently, some researchers combined PPy with highly conductive materials like reduced graphene oxide (rGO) and activated carbon to overcome these problems [46]. For example, Xu et al. [41] used PPy as an intermediate to prepare a graphene-based supercapacitor, which performs high electrochemical stability during

continuous compression and release cycles under the maximum compressive ratio of 80 %. Another study by Dang et al. [4] prepared graphene/polypyrrole electrode materials via electrochemical codeposition and reduction. In addition to expanding the material's net contact area, the porous electrode actively aided in the electrolyte ions' diffusion efficiency. As a result, the 0.2-rGO/PPy electrode produced using the deposition solution containing 0.2 mg•mL<sup>-1</sup> of GO attained a maximum capacitance of 1091.2 mFcm<sup>-2</sup> at 1 mAcm<sup>-2</sup>. At 10 mA•cm<sup>-2</sup>, the 0.2-rGO-PPy retained a capacitance of 78.4 %. Specifically, the supercapacitor based on 0.2-rGO-PPy demonstrated a stack capacitance of up to 28.3F•cm<sup>-3</sup>. Moreover, the supercapacitor demonstrated remarkable mechanical pliability, maintaining 93.3 % of its capacitance even when bent 180 degrees.

Herein, a 3D compressible PCF-rGO-Ppy//rGO electrode was prepared via grafting rGO-PPy synthesized from hydrothermal method on the skeleton of PCF through simple dip coating. The combination of double-layer carbon materials from PCF and rGO not only ensured high capacitance but also greatly improve the cycling stability and rate performance of the electrode. In particular, the outer PCF provided continuous conductive network, which makes up the lack of electronic conductivity caused by the partial accumulation of PPy. Meanwhile, the intrinsic toughness and elasticity of the PCF and PPy made the structure of electrodes avoid collapsing under a high compressive strain. Based on PCF-rGO-ppy//rGO asymmetric electrodes, a highly compressible supercapacitor device is assembled, which can maintain more than 98.89 % of the capacitance after 200 times compression and release cycles under a high compression of 80 %.

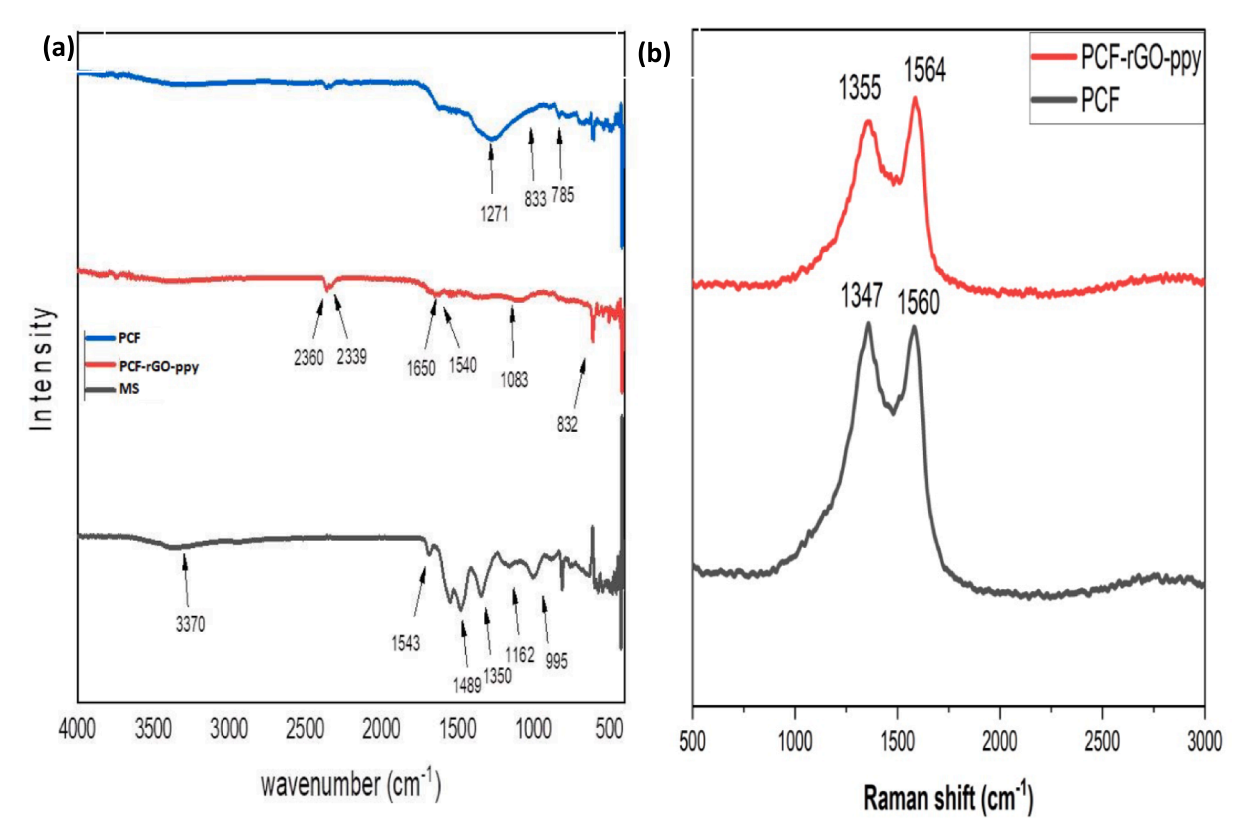


Fig. 2. (a) FTIR and (b) Raman spectra of MS, PCF, PCF-rGO-ppy.

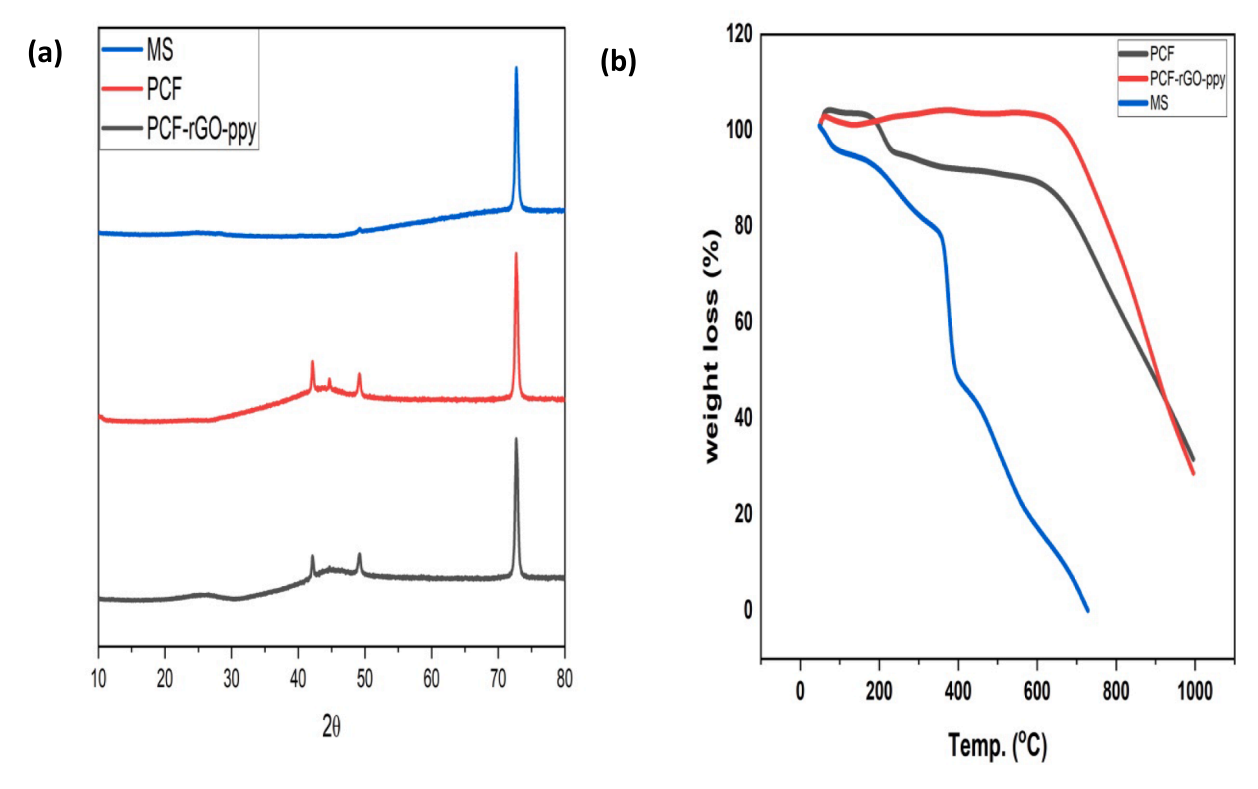


Fig. 3. (a) XRD and (b) TGA spectra of MS, PCF, PCF-rGO-ppy.

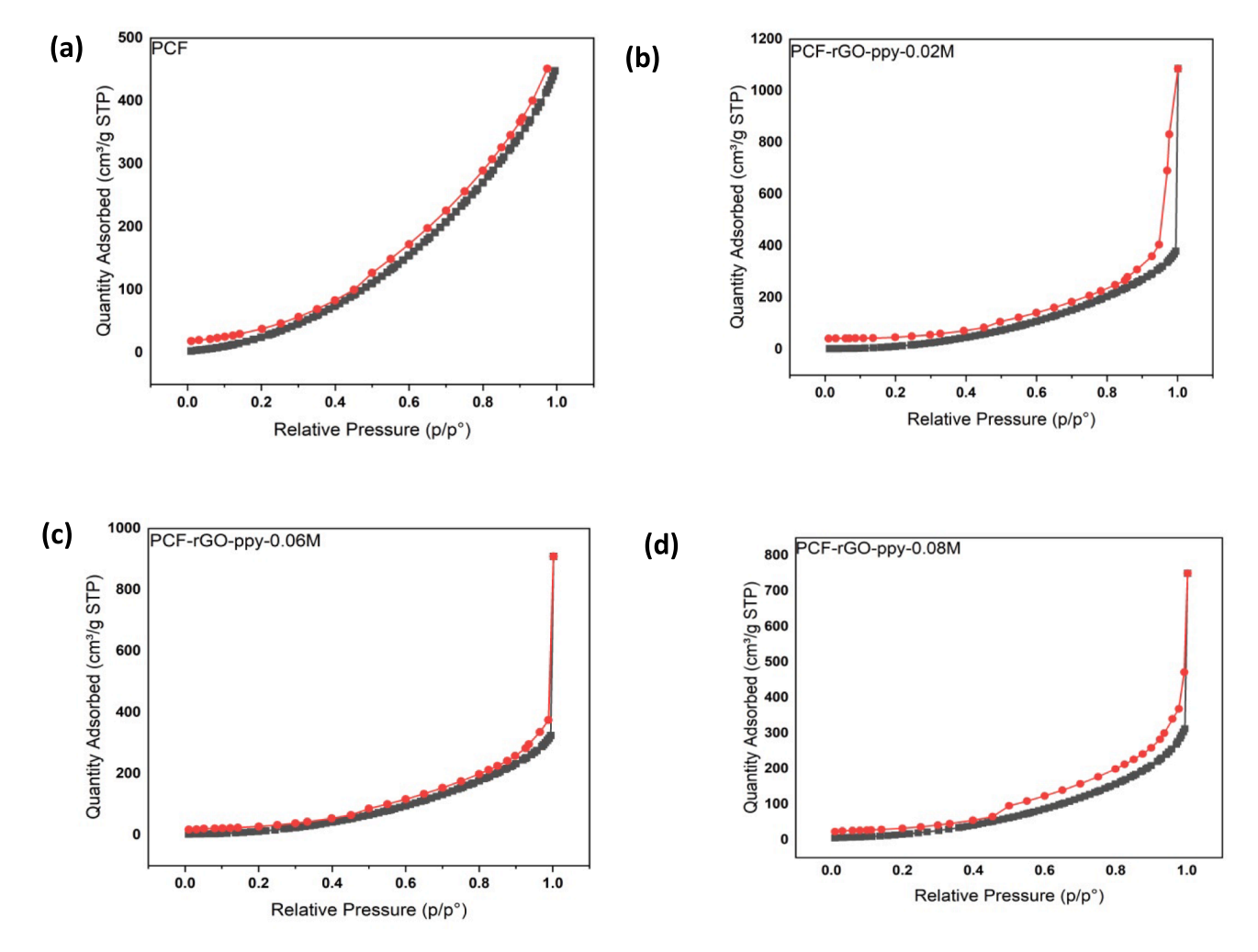


Fig. 4. N2 adsorption/desorption isotherms at 77 K of PCF and PCF-rGO-ppy at different concentrations (a) PCF (b) 0.02 M (c) 0.06 M and (d) 0.08 M.

#### 2. Experimental section

### 2.1. Preparation of PCF-rGO-ppy electrode

The rGO dispersion was obtained using a modified Hummer process [12], followed by acidification with  $\rm H_2SO_4$  and  $\rm HNO_3$  to obtain acidified rGO, then the rGO dispersion was mixed with ppy and treated hydrothermally at 120 °C to obtain rGO-ppy nanocomposite. To obtain the PCF, the MS was carbonized in a tubular furnace at a 150 °C for a holding time of 1hr at 3 °C min $^{-1}$ . The PCF (1  $\times$  1  $\times$  1 cm $^{3}$ ) was fully immersed in a linker for about 30mins and then acidified rGO dispersion (2 mgmL $^{-1}$ ) and dried at 70 °C to obtain the PCF-rGO-ppy sample, then the obtained sample was cleaned with deionized water and dried for 3 h. As a control sample, PCF-rGO was prepared by coating rGO on the PCF without ppy. The specific capacitance, energy density and power density were calculated using the formula:

$$C_A = 4I\Delta t/\Delta V_A \tag{1.1}$$

$$E = 1/7200C_A(\Delta V)^2 (1.2)$$

$$P = E/\Delta t \tag{1.3}$$

## 2.2. Characterizations and electrochemical measurements

A field emission scanning electron microscope (FESEM; Hitachi SU-8000) was employed to detect the morphology of the samples. Fourier transform infrared spectrometer (IFS-85 FTIR spectrometer) was used to

investigate the functional groups contained in the materials. The structural information was measured by a laser confocal Raman spectroscopy (Renishaw in Via) and X-ray diffraction (XRD) (PANalytical X'pert-Pro MPD PW 3040), operated at Cu-K  $\alpha$  radiation ( $\lambda=0.15406$ nm). The diffractogram was scanned at a scan rate of  $2^{\circ}$  min $^{-1}$ . The thermal stability was measured using Metter-Toledo thermogravimetric analyzer and the stress-strain tests of the samples were conducted on an electronic universal testing machine (Instron 8874). N2 adsorption-desorption isotherms were determined on a Micrometrics ASAP 2020 instrument at 77 K for the measurement of specific surface area and pore size distribution. Elemental analysis of PCF-rGO-ppy was conducted on an Ulvac PHI (PHIVersaProbe4) X-ray photoelectron spectrometer (XPS) (Shimadzu, Japan). The electrochemical characteristics of the samples were examined using a two-electrode system with the PCF-rGO-ppy as the cathode and rGO as anode electrode. The electrochemical performances were recorded by an Autolab PGSTAT204/ FRA32 electrochemical workstation.

#### 3. Results and discussion

Nickel foam with high porosity and large surface area was used as the substrate to ease the flow of electric current in the supercapacitor device. The PCF-rGO-ppy was used as the compressible electrode (cathode) and rGO was used as the anode. The 3D porous network of the PCF is constituted by smooth branched fibers (Fig. 1a and b), which owns sufficient space for the compressive deformation [30,39]. Fig. 1c and d are FESEM images of the PCF-rGO electrode, which clearly show that

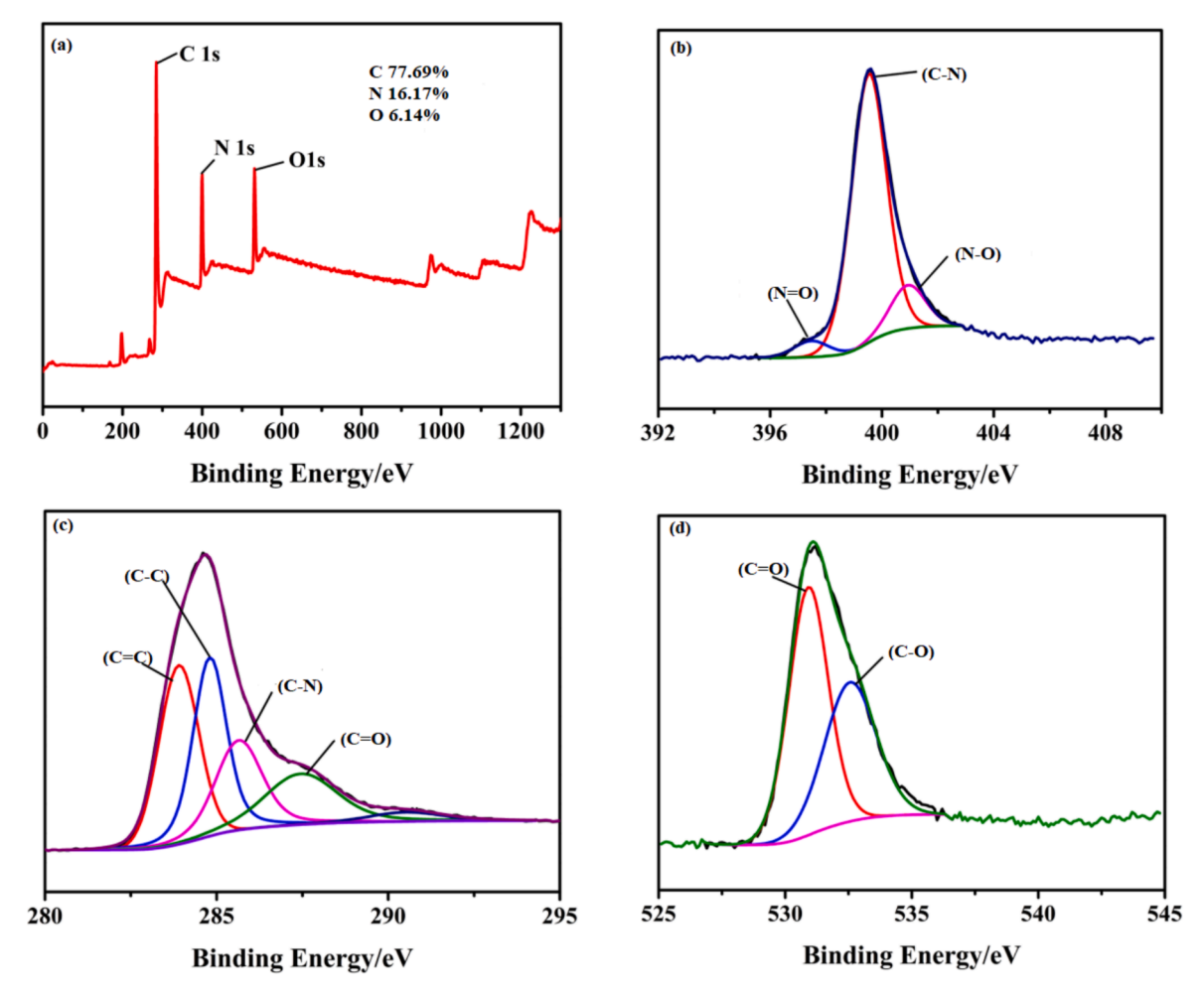


Fig. 5. Full XPS spectrum of PCF-rGO-ppy (a); survey spectrum (b) High-resolution XPS spectra of N 1 s (c), C 1 s (d) and O1s.

numerous flaky rGO-ppy is painted on the PCF skeleton. Fig. 1f and g shows the FESEM of rGO-PPy affirming ppy is anchored on the rGO sheets through a  $\pi\text{-}\pi$  stacking interaction. Unfortunately, slight local accumulation of PPy on the rGO surface can pose a threat to electron conduction as shown in Fig. 1g, which the outer carbon network sheets on the PCF can strike-out by forming a continuous conductive network, which makes up the lack of electronic conductivity caused by the partial accumulation of PPy.

The FTIR and Raman spectroscopy were used to analyze molecular structures and functional groups of these samples, and the results are displayed in Fig. 2a and b. As can be seen, the MS exhibits characteristic peaks of 1543 cm<sup>-1</sup>, 1489 cm<sup>-1</sup>, 1350 cm<sup>-1</sup>, 1162 cm<sup>-1</sup>, and 995 cm<sup>-1</sup>, which represent triazine ring structure, C-N of amino, and C-O of methylol [23]. In addition, a large and broad peak at 3370 cm<sup>-1</sup> is a superposition of stretching vibration of O-H (hydroxyl group) and N-H (amino and imino) in Melamine sponge. After carbonization, the FTIR spectrum of PCF showed peaks around 1271 cm<sup>-1</sup>, 883 cm<sup>-1</sup>and 785 cm<sup>-1</sup> represent for C-O, C-O, and O-H of carboxyl or carbonyl, respectively while in the spectrum of PCF-rGO-ppy, the peaks around 2360 cm<sup>-1</sup>, 2339 cm<sup>-1</sup>, 1650 cm<sup>-1</sup>, 1540 cm<sup>-1</sup>, 1082 cm<sup>-1</sup> and 832 cm<sup>-1</sup>. The carboxyl groups can be ionized in an aqueous solution and transform into functional groups with opposite charges, which binds rGO to the PCF through electrostatic interaction. Compared with PCF, PCFrGO-ppy possesses a peak around 1082 cm<sup>-1</sup>, which can be ascribed to the in-plane deformation of C-H and tensile vibration of C-C in the pyrrole ring, indicating that PPy is successfully grafted on PCF. The Raman spectrum of PCF exhibits two intensive peaks of 1564 cm<sup>-1</sup> and 1355 cm<sup>-1</sup> corresponding to D and G bands. It can be observed from the

spectrum of PCG-rGO-ppy, peaks related to rGO and PCF are maintained at 1560 cm<sup>-1</sup> and 1347 cm<sup>-1</sup>. A distinct peak of 1046 cm<sup>-1</sup> appears in the FTIR spectrum of PCF-rGO-ppy, representing C–H vibration of pyrrole ring [32], which proves the successful preparation of PPy. In addition, PCF-rGO-ppy possesses a strong peak at 1540 cm<sup>-1</sup>, which is a superposition of the C–C backbone tension of PPy and the D band of rGO [28]. And the peak of 1083 cm<sup>-1</sup> can be attributed to the stretching vibration of C-N (PPy) and G band of rGO. (Fig. 3a and b).

The  $N_2$  adsorption–desorption analysis was performed to further determine the porosity of the PCF and PCF-rGO-ppy. The PCF showed a typical microporous type III isotherm but with the introduction of rGO-ppy, mesopores were introduced. The main role of the mesopore is to improve the rate performance of the materials. The specific surface area reduced from  $99\ m^2/g$  to  $44.18\ m^2/g$  depending on the concentration of rGO-ppy loaded on the porous foam. This indicates that the rGO materials have successfully been loaded onto the porous foams by filling up the pores on the materials hence reduces the surface area.

The structural property of MS, PCF and PCF-rGO-ppy was also studied using XRD and the thermal properties studied by thermogravimetric analysis (TGA). XRD spectra showed peaks attributed to MS, PCF and PCF-rGO-ppy showing the successful synthesis of PCF and PCF-rGO-ppy from MS. The TGA curve of MS showed several weight loss at different temperatures which proved the thermal instability of the material. After carbonization to produce PCF, the PCF showed better stability as the temperature rose of 1000  $^{\circ}$ C. PCF-rGO-ppy showed far better stability and remained thermally stable even at high temperature of 750  $^{\circ}$ C because of the presence of the nanocomposite grafted on the PCF.

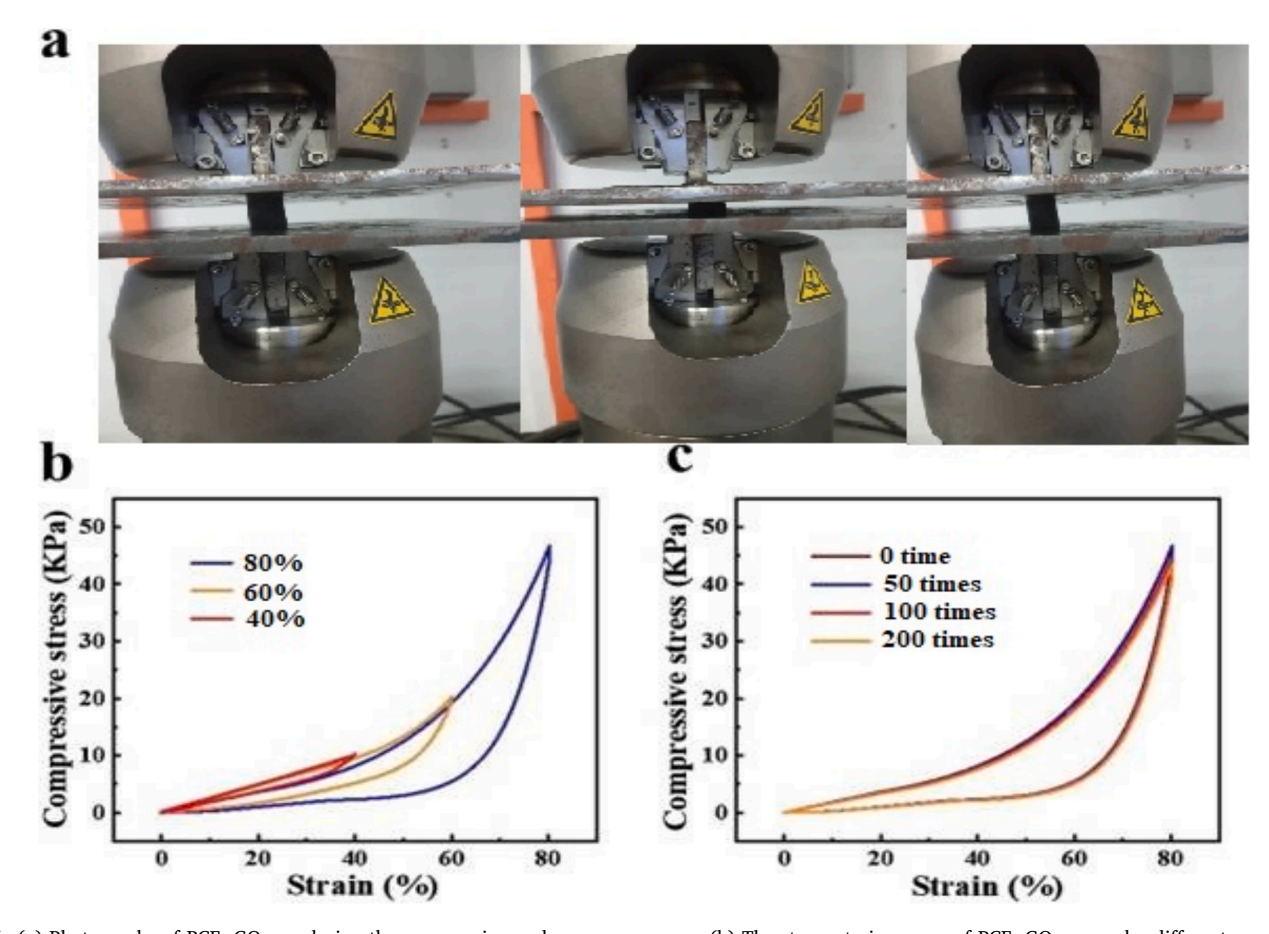


Fig. 6. (a) Photographs of PCF-rGO-ppy during the compression and recovery process. (b) The stress–strain curves of PCF-rGO-ppy under different compressive strain. (c) The stress–strain curves after different compressing-recovering cycles.

In addition to improving the rate performance and specific capacity, the accessible surface area, appropriate pore size distribution, and well-developed nanostructure are advantageous for electrolyte penetration and quick ions diffusion as presented in Fig. 4(a–d).

The mechanical characteristics of the PCF-rGO-ppy electrode were tested during the compressing and recovering process (Fig. 6a). As shown in Fig. 6b, The PCF-rGO-ppy exhibits a typical behavior of porous sponge. At low strain (< 10 %), a linear relationship is observed between strain and stress, showing the characteristic of elastic behavior. A plateau appears at intermediate strain (10 %  $\sim$  50 %), indicating that the skeleton of the sponge is squeezed. At high strain (> 50 %), the stress rises rapidly with the increase of strain due to the plastic stiffening (Q. [45]. The curve returns to the origin after every stress-strain cycle, indicating that the shape and size of the electrode can completely recover. It is worth noting that many of the reported compressible electrodes have lost elasticity or even fractured at 80 % compressive strain [40]. In addition, the stress-strain curve of the PCF-rGO-ppy almost coincides with the original curve after 200 times compressingrecovering cycles (at a high strain of 80 %), demonstrating that the PCFrGO-ppy electrode has highly durable and reversible properties. (Fig. 6c).

Fig. 5 show that the PCF-rGO-ppy material constitutes mainly O 1 s, N 1 s and C 1 s signals. The surface atomic percentages by mass of C, O and N in the material are 77.69 %, 16.17 % and 6.14 %, respectively as shown is the survey spectrum from Fig. 6a. In Fig. 5b, The N spectrum showed the existence of N=O at 397.59 eV, C=N at 399.80 eV and N=O at 401.20 eV. This is in concordance with the N<sub>1s</sub> peak of PPy in Fig. S2b, indicating that rGO-PPy is successfully anchored on the surface of the PCF. In Fig. 5c, the C<sub>1s</sub> spectrum shows the C=C chemical state of 283.9 eV, C=C of 284.8 eV, C=N/C=O of 285.69 eV, and the chemical state of

C=N/C=O of 287.44 eV coexist. The peak near 290.58 eV is the satellite peak of  $C_{1s}$ , reflecting molecular structure information (It may be the pipi\* transition of the benzene ring) [6]. This is consistent with the  $C_{1s}$  peak information of rGO and PPy in Fig. S1c and Fig. S2c, respectively. The  $O_{1s}$  is shown in Fig. 5d as 530.87 eV C=O and 532.28 eV C=O chemical states coexist.

The amount of rGO-ppy nanocomposite loaded on the PCF was optimized since the nanocomposite was the major provider of the capacitance. The electrochemical performance of the electrodes with different concentrations of the nanocomposite was tested. In Fig. 7a, the cyclic voltammetry (CV) curve of the PCF-rGO-ppy-0.02 M electrode has a large enclosed area representing high specific capacitance. A small difference can be observed from the CV curve of PCF-rGO-ppy-0.06 M, indicating that the electrode almost the same capacitance with the PCFrGO-ppy-0.02 M. The encapsulated area of the CV curve of PCF-rGOppy-0.08 M is very small because the loading of rGO-PPy is too much to provide considerable space for the movement of ions to provide high capacitance. Fig. 7b displays galvanostatic charge/discharge (GCD) curves of all electrodes. The GCD curve of the electrodes are all symmetric linear, demonstrating that this electrode possesses a good charge/discharge character. By contrast, the larger iR drop and shorter discharge time of PCF-rGO-ppy-0.08 M electrode represent the inferior electrochemical performance. For analyzing the rate capabilities of samples in detail, the specific capacitances of samples at multiple current densities were calculated. When the current density increases from  $0.5 \text{ A g}^{-1}$  to  $5 \text{ Ag}^{-1}$ , 83.8 % of the specific capacitance of PCF-rGO-ppy-0.02 M is maintained. As shown in Fig. 8d, the capacitance retention of PCF-rGO-ppy-0.02 M is 98.89 % after 10,000 cycles, which is higher than that of PCF-rGO-ppy-0.06 M and PCF-rGO-ppy-0.08 M which are 93.57 % and 90.91 % respectively. The Ragone plot for of PCF-rGO-

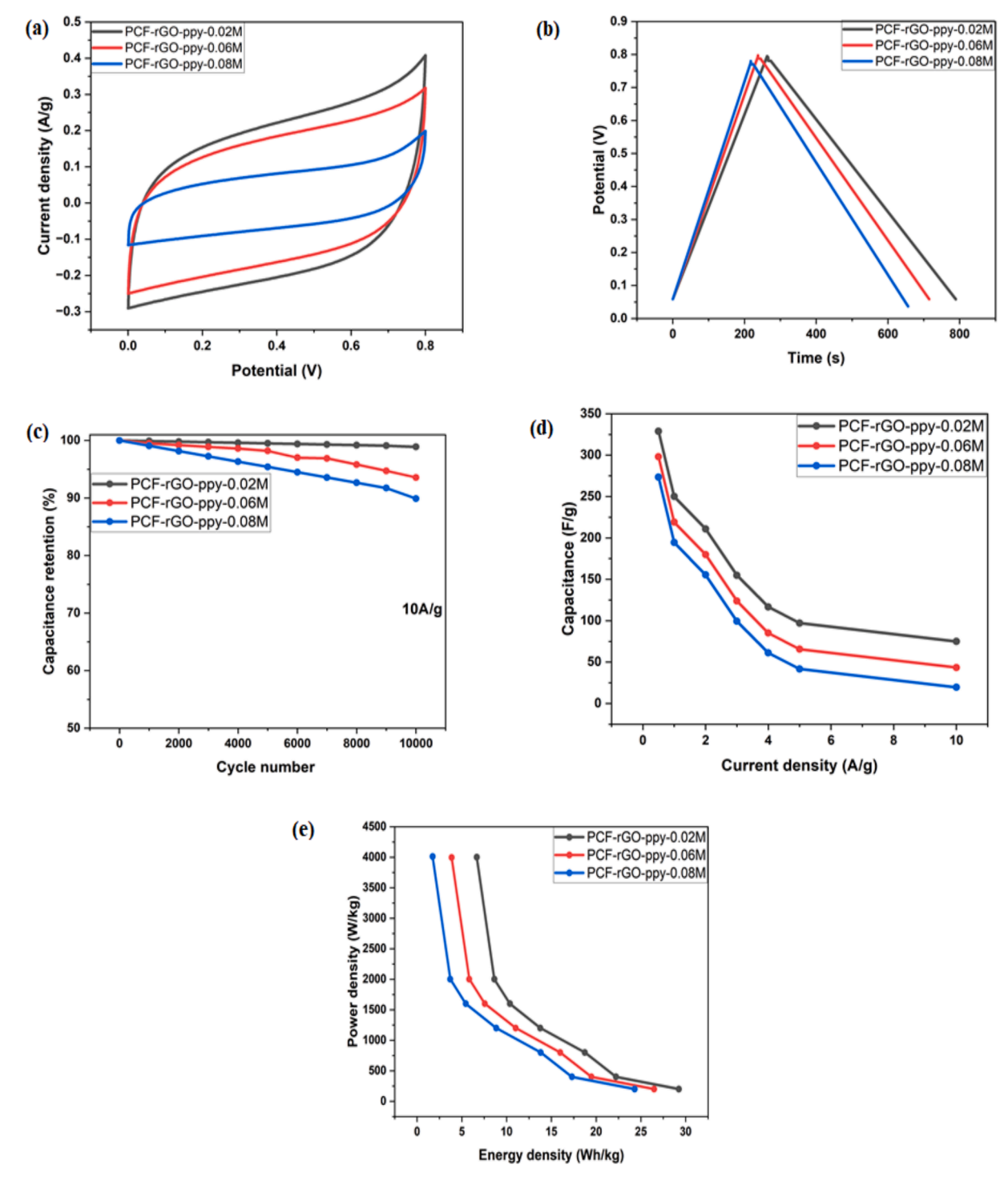


Fig. 7. (a) CV curves, (b) GCD curves, (c) specific capacitance at various current densities and (d) cycling stability (e) Ragone plot of PCF-rGO-ppy@ 0.02 M rGO-ppy, PCF-rGO-ppy@ 0.06 M rGO-ppy and PCF-rGO-ppy@ 0.08 M rGO-ppy electrodes.

ppy@ 0.02 M rGO-ppy, PCF-rGO-ppy@ 0.06 M rGO-ppy and PCF-rGO-ppy@ 0.08 M rGO-ppy electrodes is illustrated in Fig. 8e. Therefore, the PCF-rGO-ppy-0.02 M electrode exhibited optimal electrochemical performance

The electrochemical performance of PCF-rGO and PCF electrodes were measured and used as control. The FESEM images (Fig. 1) of rGO and PCF reveal the micromorphology of the materials. Fig. 8a shows the cyclic voltammetry (CV) curve of PCF, PCF-rGO and PCF-rGO-ppy electrodes at  $10 \text{mVs}^{-1}$ . The electrodes showed large enclosed area representing high capacitance. The voltammogram showed a distorted

rectangular shape which shows the effect of electric double layer capacitance (EDLC). The encapsulated area of PCF, PCF-rGO and PCF-rGO-ppy are similar because these materials are both carbon-based materials. PCF-rGO-ppy on the other hand showed a more distorted CV curve and this is due to the presence of ppy which contributes to the electrochemical performance through pseudocapacitance. Fig. 8b shows the galvanostatic charge/discharge (GCD) curves of all electrodes at 0.5A/g. The GCD curves of the electrodes is symmetric linear, demonstrating that the electrodes possesses good charge/discharge character. By contrast, the larger iR drop and shorter discharge time of PCF which

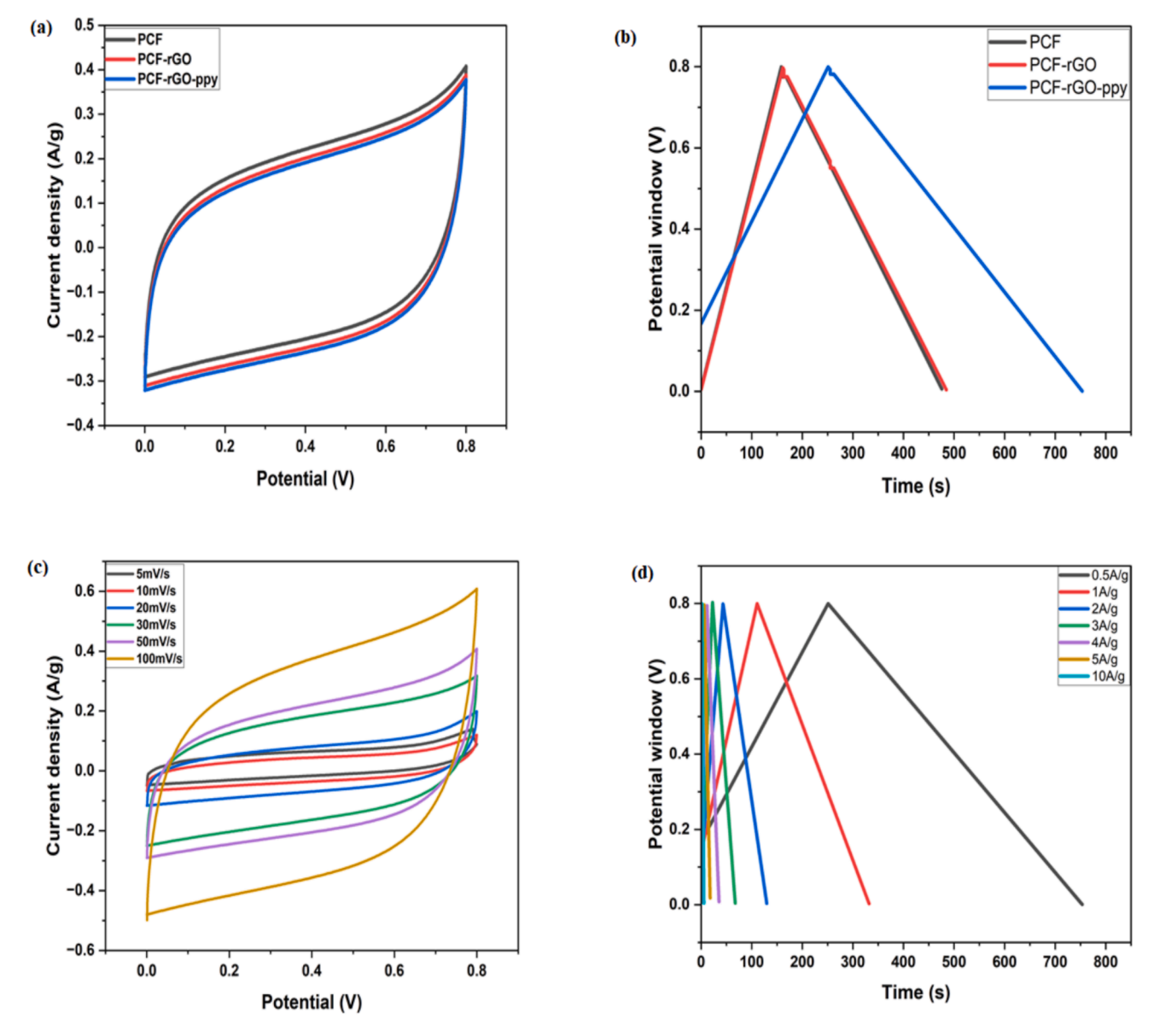


Fig. 8. (a) CV curves of the PCF-rGO-ppy, PCF-rGO and PCF electrode. (b) GCD curves of PCF-rGO-ppy, PCF-rGO and PCF electrodes. (c) CV curves and (d) GCD curves of the PCF-rGO-ppy electrode.

is almost the same with that of PCF-rGO represent inferior electrochemical performance. For the purpose of analyzing the specific capacitance of the electrodes in details, the specific capacitances of the samples at different current densities were calculated. When the current density was increased from 0.5A/g to 10A/g, a certain percentage of the specific capacitance was maintained for all the electrodes. The Nyquist plot of the electrode materials was displayed in Fig. 12. The charge transfer resistance related to the semicircle in the high frequency region of PCF is a bit larger than that of PCF-rGO which is also almost the same value for PCF-rGO-ppy. Even with the presence of ppy which leads to increase in charge transfer resistance and sluggish ion transfer kinetics. But with the presence of double layer of carbon materials from PCF and rGO, the charge transfer resistance of the PCF-rGO-ppy electrode was small which shows the advantage of using PCF as the 3D substrate for the compressible supercapacitors and can provide avenue for high ion transfer. As shown in Fig. 10d, the capacitance retention of the electrode materials after 10,000 cycles. The retention capability of PCF, PCF-rGO and PCF-rGO-ppy were, 85.89 %, 88.89 % and 98.89 % respectively. This also shows the effect of the double layer of carbon materials as it related to capacitance retention.

In the composition of the PCF-rGO-ppy electrode, the highly conductive porous carbon material becomes a good substrate for loading of composite materials with EDLC, pseudocapacitive or hybrid characteristics to fabricate compressible supercapacitors. The CV curve of PCF (Fig. 8a) can maintain a quasirectancgular shape even at  $100 \, \mathrm{mVs}^{-1}$  implying that the PCF possesses excellent rate performance. However, the small current response represents low capacitance of the PCF electrode which suggests that the charge transfer capacity of the PCF is not sufficient enough making it necessary to bring in the rGO-ppy nanocomposite with high pseudocapacitive properties in order to increase the capacitance of the compressible electrodes.

Compared with PCF and PCF-rGO, the CV of the PCF-rGO-ppy possesses higher current response at  $10 \text{mVs}^{-1}$  (Fig. 8c), demonstrating that the capacitance is greatly increased by the introduction of the hydrothermally synthesized rGO-ppy nanocomposite. The higher electrochemical performance can therefore be said to be from the combination of the double layer of carbon materials and the pseudocapacitance from ppy.

Meanwhile, the GCD curve of the PCF-rGO-ppy electrode display longest discharging time, indicating that the material has the highest

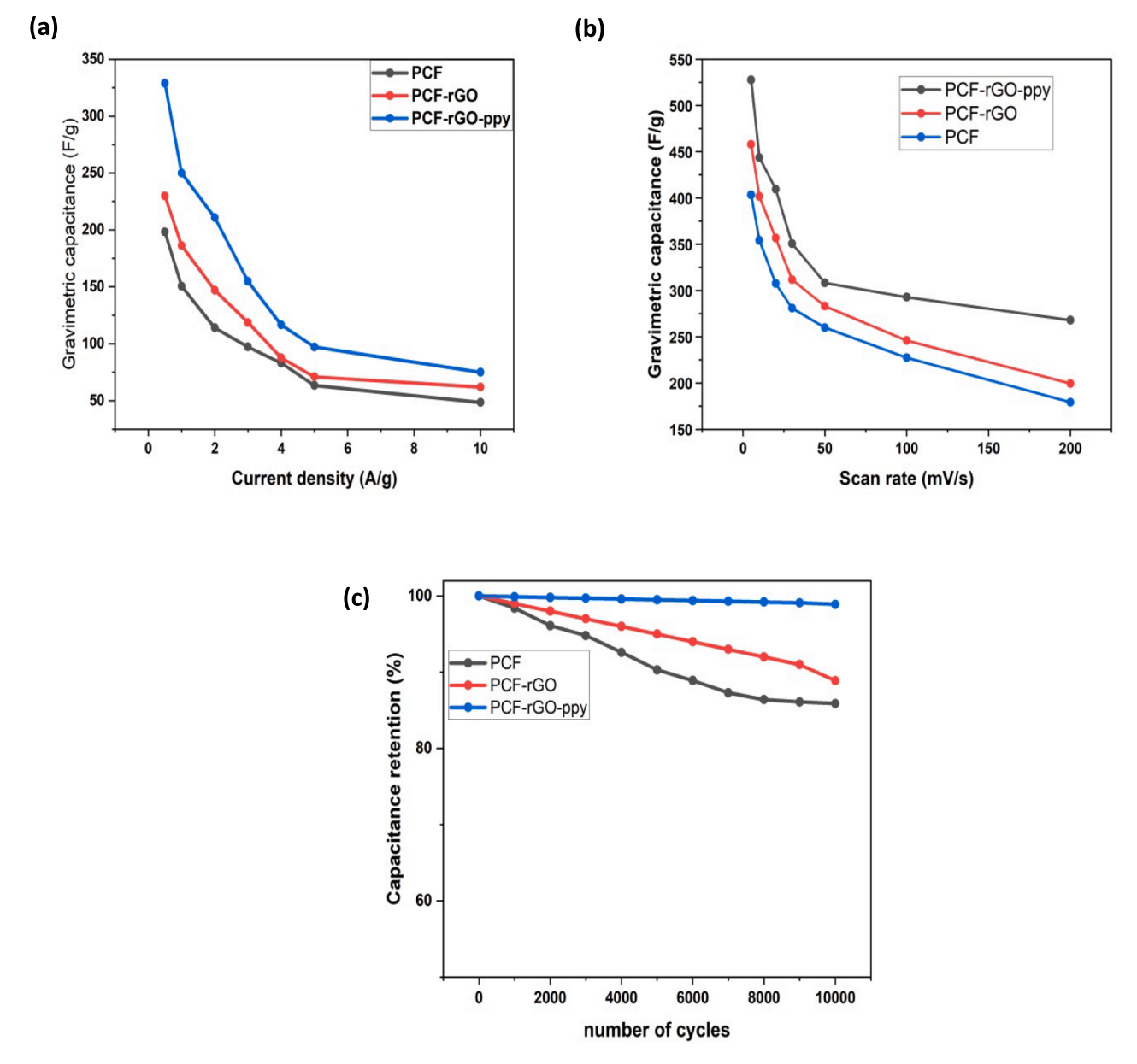


Fig. 9. (a) Gravimetric capacitance against current density (A/g) (b) gravimetric capacitance against scan rate (mV/s) and (c) cycling stability of PCF, PCF-rGO and PCF-rGO-ppy electrodes.

specific capacitance. The high electric conductivity of the PCF-rGO-ppy electrode at various current densities is shown in Fig. 8d, all the curves showed symmetric shapes indicating ideal capacitance characteristics. The gravimetric and volumetric capacitances of all the samples are displayed in Fig. 9a and 9b.

The gravimetric capacitance of the PCF-rGO-ppy//rGO device was 328.91 at 0.5  ${\rm Ag}^{-1}$ , which is superior to 230F  ${\rm g}^{-1}$  of the PCF-rGO//rGO and 198.29F  ${\rm g}^{-1}$  of the PCF//rGO supercapacitor device. When the current density increases to 10 A  ${\rm g}^{-1}$ , the capacitance of the PCF-rGO-ppy device was maintained at 74.99F  ${\rm g}^{-1}$ .

In the high-frequency region, the intercept at the real axis is related to the resistance of electrolyte and components ( $R_s$ ). According to the fitting results of the equivalent electrical circuit, the  $R_s$  of PCF-rGO-ppy is the smallest (1.43  $\Omega$ ). The charge-transfer resistance ( $R_{ct}$ ) corresponds to the semicircle, and the  $R_{ct}$  of PCF-rGO-ppy, PCF-rGO and PCF

electrodes are  $4.02\,\Omega,\,6.01\,\Omega$  and  $6.06\,\Omega,$  respectively. The PCF-rGO-ppy electrode possesses the smallest value, suggesting that the double layer of carbon materials can effectively improve the charge-transfer rate. At the low-frequency region, the slope of plots can be attributed to ions diffusion. The slope of the line of PCF-rGO-ppy is much larger than PCF-rGO and PCF, and it is nearly perpendicular to the imaginary axis, indicating that PCF-rGO-ppy electrode has ideal capacitance characteristics. The  $R_s$  and  $R_{ct}$  value were determined after 10000th cycle to determine the degree of contact between the electrode material and the current collector after several cycles. The increase of  $R_{ct}$  is also responsible for the decrease of the energy density of the device. After 10,000 cycles, very little change was observed for  $R_s$  (from 2.45  $\Omega$  to 2.90  $\Omega$  for PCF/rGO, 2.40  $\Omega$  to 2.85  $\Omega$  for PCF-rGO/rGO and 1.43 to 1.93  $\Omega$  for PCF-rGO-ppy/rGO), but an apparent increase of  $R_{ct}$  (from 6.06  $\Omega$  to 27.20  $\Omega$  for PCF/rGO, 6.01  $\Omega$  to 26.70  $\Omega$  for PCF-rGO//ppy

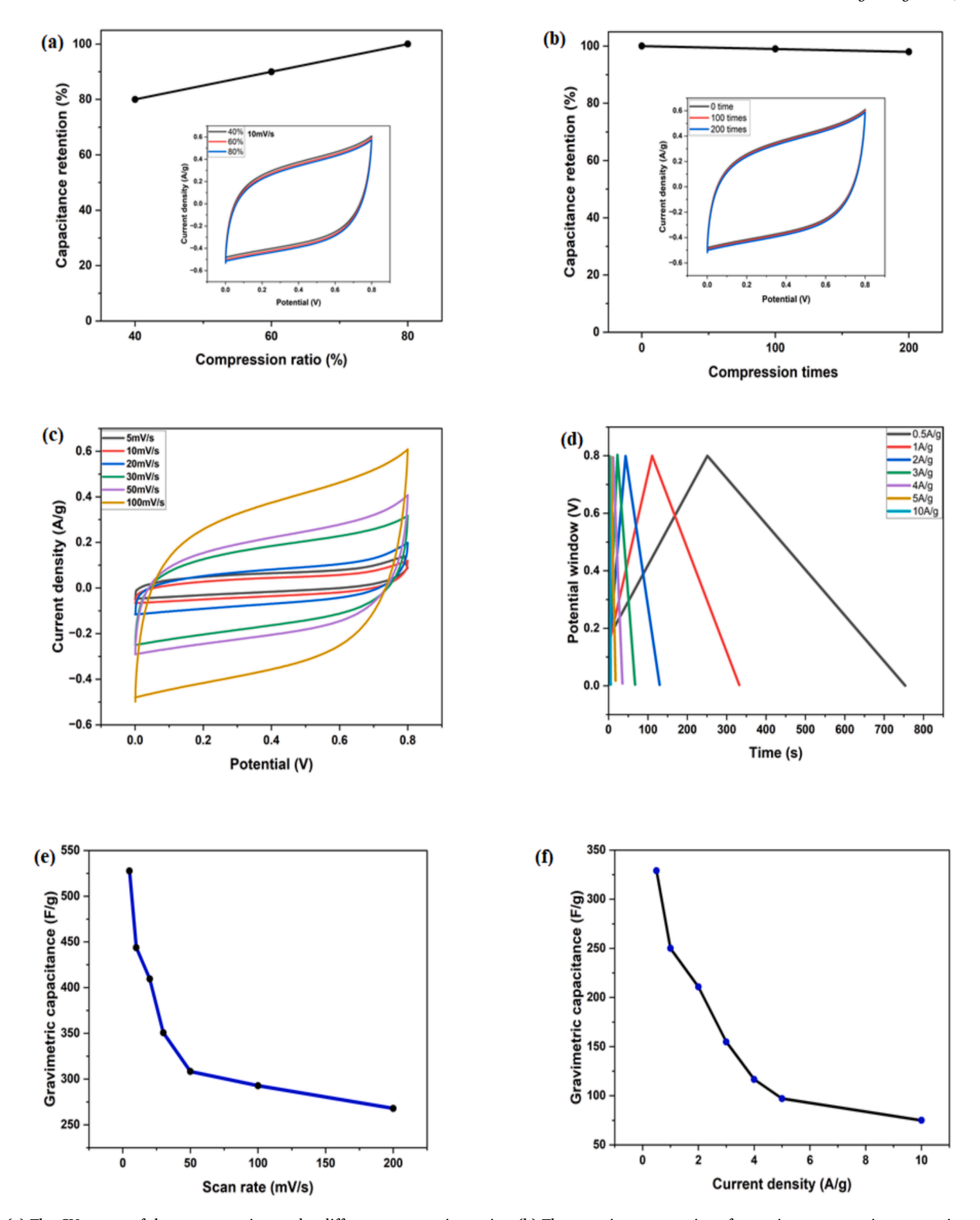


Fig. 10. (a) The CV curves of the supercapacitor under different compression ratios. (b) The capacitance retention after various compressing-recovering cycles. (c) The CV curves, (d) the GCD curves, (e, f) Gravimetric capacitance at various scan rates and current densities.

and 4.02 to 25.26  $\Omega$  for PCF-rGO-ppy//rGO) was observed as shown in Fig. 11 [5].

The introduction of the double layer of carbon materials makes the specific capacitance of the PCF-rGO-ppy electrode be maintained 98.89 % after 10,000 cycles, which is much larger than 88.89 % of the PCF-rGO electrode and 85.89 % of the PCF electrode (Fig. 9c). The excellent electrochemical performance of the PCF-rGO-ppy electrode is attributed to two aspects. On the one hand, the 3D highly porous

structure of PCF provides a short path for ion transport [29]. On the other hand, rGO forms a complete conducting network and increases the electronic conductivity. Compared with recently reported compressible electrodes, the PCF-rGO-ppy electrode has advantages in maintaining the excellent electrochemical performance under an ultrahigh compressive strain (Table 1). Compared with conventional supercapacitors, all-solid-state compressible supercapacitors are more suitable as energy storage devices for wearable electronic appliances

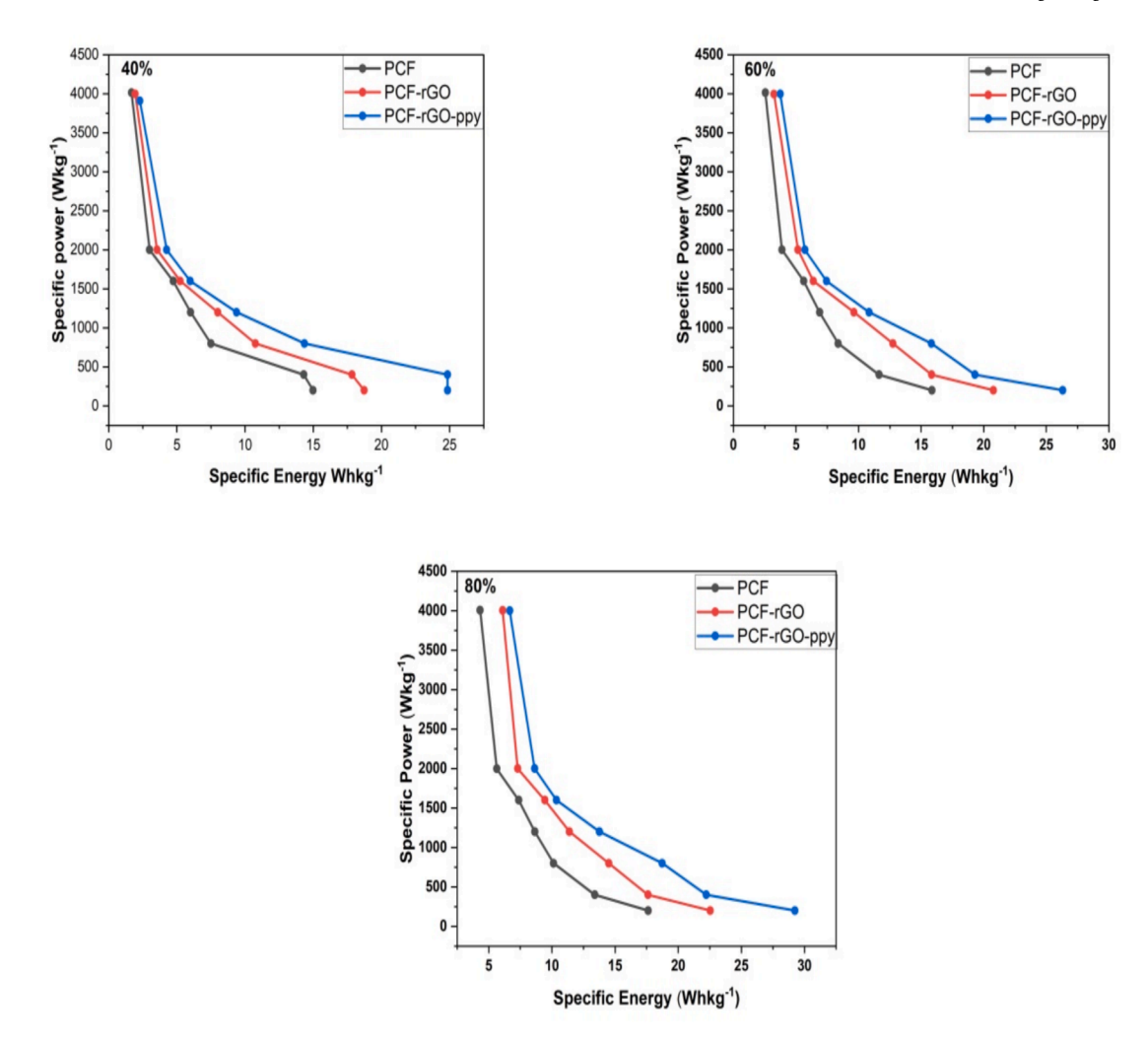


Fig. 11. (a) Ragone plot for PCF, PCF-rGO and PCF-rGO-ppy @ 40% compression ratio (b) Ragone plot for PCF, PCF-rGO and PCF-rGO-ppy @ 60% compression ratio (c) Ragone plot for PCF, PCF-rGO and PCF-rGO-ppy @ 80% compression ratio.

[10,42,44]. Herein, an all-solid-state asymmetrical compressible supercapacitor consists of one PCF-rGO-ppy as the cathode and rGO as the anode electrodes with KCl/PVA gel as the electrolyte. Fig. 10a displays the CV curves of this supercapacitor at various compression ratios. The specific capacitance rises slowly as increase of the compressive strain, and the capacitance under 80 % compressive strain is slightly larger than the capacitance under 60 % and 40 % compressive strain respectively. The reason for this phenomenon is that, under the high compressive strain, the decrease of the electrode thickness reduces the moving distance of ions, and the close contact of active materials is favorable for charge transfer. Besides, Fig. 11b shows the capacitance retention of the supercapacitor after 0, 50, 100 and 200 times compressing-recovering cycles under the compressive strain of 80 %, which shows that 97.99 % of capacitance can be maintained after 200 cycles. The results of the CV and the GCD tests show that the all-solidstate supercapacitor possesses excellent capacitance characteristics (Fig. 10c and 10d). The specific capacitance was calculated according to GCD tests. The result of the GCD test shows that the gravimetric capacitance is 328.91F g<sup>-1</sup> at 0.5 Ag<sup>-1</sup>. This value is competitive among recently reported compressible supercapacitors, such as supercapacitors based on nitrogen-doped porous graphene framework (65.5F g<sup>-1</sup> at 3  $mAcm^{-2}$ ) [37,38] and PPy-CFs/MS/PPy-CFs (95.6F  $g^{-1}$  at 0.05 mAcm<sup>-1</sup>) [1]. After 10,000 cycles, the capacitance retention at different compression rate was 93.99 %, 96.17 % and 98.89 % at 40 %, 60 % and 80 % compression rates (Fig. 11a). The Ragone plot (Fig. 11b) was calculated by the GCD, the highest power density is 4004.98Wkg<sup>-1</sup> and

the energy density is 17.63Wh kg<sup>-1</sup>.

#### 4. Conclusion

In this study, an excellent compressible electrode was designed and synthesized by grafting rGO-PPy on the skeleton of PCF. The PCF-rGO-ppy//rGO device possesses a high gravimetric capacitance of 328.91F g<sup>-1</sup> and desirable cycling stability (98.89 % after 10,000 cycles). The all-solid-state supercapacitor constructed by PCF-rGO-ppy electrodes possesses gravimetric capacitance of 328.91F/g under the 80 % high compressive strain and excellent capacitance retention of 97.48 % after 200 stress–strain cycles. In addition, the highest power density and energy density of the supercapacitor are 4004.98 Wkg<sup>-1</sup> and 17.63 Whkg<sup>-1</sup> respectively. Therefore, this study offers new insights into the field of designing and manufacturing compressible supercapacitors with both excellent electrochemical performance and mechanical properties.

#### CRediT authorship contribution statement

Balarabe El-yaqub: Writing – original draft, Methodology. Mohd Haniff Wahid: Writing – review & editing, Project administration, Funding acquisition, Conceptualization. Zulkarnain Zainal: Writing – review & editing, Supervision, Software, Resources. Abdul Halim Abdullah: Writing – review & editing. Wan Azlina Wan Ab Karim Ghani: Writing – review & editing.

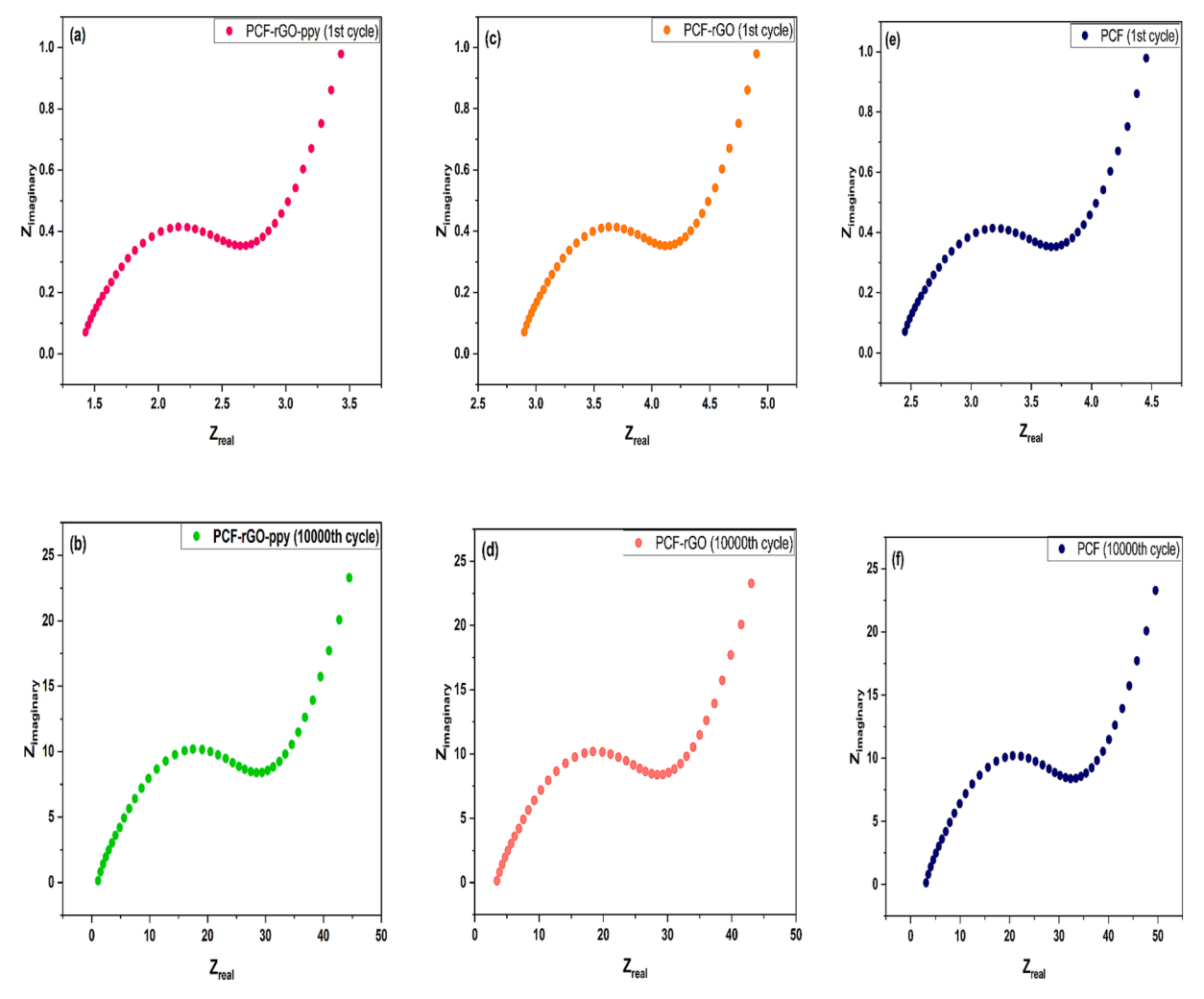


Fig. 12. Schematic diagram showing (a) Nyquist plots (1st cycle) for PCF-rGO-ppy (b) Nyquist plots (10000th cycle) for PCF-rGO-ppy (c) Nyquist plots (1st cycle) for PCF-rGO (d) Nyquist plots (10000th cycle) for PCF.

 Table 1

 Electrochemical performance of recently reported compressible electrodes.

Compressible electrode	Capacitance (F g <sup>-1</sup> )	Capacitance retention/compressive strain	Cycling stability	Ref.
Nitrogen-doped graphene aerogel (GASC)	150.0 (0.3 A g <sup>-1</sup> )	90 %/75 %	85.1 % after 10,000	[9]
Nitrogen-doped graphene aerogels (NGA)	$223 (0.2 \text{A g}^{-1})$		92 % after 2000	[33]
CNF/RGO		96 %/30 %	82 % after 5000 cycles	[18]
CNF-CNT aerogel	25 (60C)	~100 %/75 %	75 % after 400	[26]
Fe <sub>2</sub> O <sub>3</sub> /CNT sponge	297.2 (5 mV·s <sup>-1</sup> )	>90 %/70 %	60 % after 1000	[3]
CNT@PPy sponge	$376 (0.5 \text{ A g}^{-1})$	>90 %/50 %	80 % after 1000	[15]
PPy/MF	73.35 (10 mA cm <sup>-3</sup> )	>100 %/70 %	66.05 % after 5000	[20]
MF-G-PPy	$427.0 (0.5 \text{ A g}^{-1})$	>92.1 %/50 %	82 % after 5000	[14]
PAGH	$176.0 (1 \text{ A g}^{-1})$	_	86.2 % after 10,000	[21]
PPy/MS-CFs (70)	239.0 (2 mV·s <sup>-1</sup> )	~98 %/60 %	90.4 % after 10,000	[2]
RGO-PPy-Ag	447.5 (0.5 A g <sup>-1</sup> )	>100 %/50 %	96.2 % after 10,000	[43]
Graphene/MnO <sub>2</sub> aerogel	320.0 (1 A g <sup>-1</sup> )	94.4 %/90 %	78 % after 3500	[22]
G-PPy-G-MS	464.1(0.5 A g <sup>-1</sup> )	>100 %/80 %	85.4 % after 5000	[41]
NiO/MnO <sub>2</sub> /CNT Sponge	23 F/g at 0.1 A/g	=	Over 100 % after 10.000 cycles	[27]
CNT reinforced MS Sponge	6.7 F/g	_	88 % after 5000	[38]
Carbon Nanotube@Polypyrrole@MnO <sub>2</sub> Sponge	9.6 F/cm <sup>3</sup>	_	90.2 % after 1000	[15]
CNT@polypyrrole core–shell Sponge	255.4 F/g (200 mV/	_	80 % after 1000	[16]
arriepotypyrrote core stien opolige	s)		00 % tater 1000	[10]
Nickel – Cobalt Sulfide Nanosheets on Carbon Sponge electrode	$1093 \text{ F/g at } 0.5 \text{ A g}^{-1}$	>60 %/70 %	83 % after 8000 cycles	[17]
CNT-PDMS Sponge Supercapacitor	13.82 mF cm <sup>-3</sup>	_	98.44 % after 3000 cycles.	[31]
Polydopamine/melamine sponge	365.6 Fg <sup>-1</sup> at 0.5Ag <sup>-1</sup>	-	86.6 % after 10000cycles	[24]
PM-H	$314.0 \text{ Fg}^{-1} (1\text{A/g})$	-	79.3 % after 3000 cycles, 2 A/g	[8]
PANI/SA/GO	457.0Fg <sup>-1</sup> (0.5A/g)		88.1 % after	[13]
	437.0Fg (0.3A/g)	_	(3000 cycles,2A/g)	[13]
			(3000 Cycles,2A/g)	
PANI-HA	$369.0 \text{ Fg}^{-1}(0.5 \text{ A/g})$	-	83.9 % after(10,000 cycles, 3 A/g)	[19]
PVA/PANI/CNT/ATMP	$389.5 \text{ Fg}^{-1} (0.5 \text{ A/g})$	-	92.0 % after(10,000 cycles, 10 A/g)	[35]
PPA-Ag	510.0 Fg <sup>-1</sup> (0.5 A/g)	_	91.0 % after(2000 cycles, 1 A/g)	[47]
CS/PANI-2	383.7 Fg <sup>-1</sup> (0.5 A/g)	-	84.5 % after(10,000cycles, 10A/g)	[48]
PCF-rGO-ppy//rGO	$328 \text{ Fg}^{-1} (0.5 \text{A g}^{-1})$	>100 %/80 %	98.89 % after 10,000	This work

# Declaration of competing interest

The authors declare that they have no known competing financial interests or personal relationships that could have appeared to influence the work reported in this paper.

# Acknowledgement

This work has been supported by Universiti of Putra, through grant no: Geran Putra GP-IPS/2023/9746900

# Data availability

Data will be made available on request.

#### References

- [1] Y. Chang, G. Han, Y. Chang, Y. Xiao, W. Hou, W. Zhou, Flexible and compressible electrochemical capacitors based on polypyrrole/carbon fibers integrated into sponge, *J. Alloy. Compd.* 708 (2017) 1206–1215, https://doi.org/10.1016/j. jallcom.2017.03.107.
- [2] Y. Chang, N. Wang, G. Han, M. Li, Y. Xiao, H. Li, The properties of highly compressible electrochemical capacitors based on polypyrrole/melamine spongecarbon fibers, J. Alloy. Compd. 786 (2019) 668–676.
- [3] X. Cheng, X. Gui, Z. Lin, Y. Zheng, M. Liu, R. Zhan, Y. Zhu, Z. Tang, Three-dimensional α-Fe 2 O 3/carbon nanotube sponges as flexible supercapacitor electrodes, J. Mater. Chem. A 3 (42) (2015) 20927–20934.

- [4] F. Dang, Y. Cai, P. Yang, Electrodeposition of Graphene/Polypyrrole Electrode for Flexible Supercapacitor with Large Areal Capacitance, ACS Appl. Energy Mater. (2024).
- [5] H. Fei, N. Saha, N. Kazantseva, R. Moucka, Q. Cheng, P. Saha, A highly flexible supercapacitor based on MnO2/RGO nanosheets and bacterial cellulose-filled gel electrolyte, *Materials* 10 (11) (2017) 1–13, https://doi.org/10.3390/ma10111251.
- [6] M. Feng, W. Lu, Y. Zhou, R. Zhen, H. He, Y. Wang, C. Li, Synthesis of polypyrrole/ nitrogen-doped porous carbon matrix composite as the electrode material for supercapacitors, Sci. Rep. 10 (1) (2020) 1–12, https://doi.org/10.1038/s41598-020-72392-x.
- [7] M. Haciismailoglu, D. Vatansever, M. Alper, Polypyrrole–oxalate and polypyrrole–sulfate electrodes for supercapacitor applications, *Chem. Pap.* 78 (5) (2024) 3315–3329.
- [8] H. Huang, C. Li, J. Luo, J. Huang, P. Yu, L. Li, C. Xiong, Controllable synthesis of hierarchically porous polyaniline/MnO2 composite with wide potential window towards symmetric supercapacitor, Colloids Surf A Physicochem Eng Asp 654 (2022) 130199.
- [9] D. Jiang, C. Li, W. Yang, J. Zhang, J. Liu, Fabrication of an arbitrary-shaped and nitrogen-doped graphene aerogel for highly compressible all solid-state supercapacitors, J. Mater. Chem. A 5 (35) (2017) 18684–18690.
- [10] L. Jiang, Y. Li, F. Zou, D. Gan, M. Gao, L. Yuan, Q. Zhang, X. Lu, Highly self-adhesive, compressible, stretchable, all hydrogel-based supercapacitor for wearable/portable electronics, *Mater. Today Phys.* 33 (2023) 101046.
- [11] X. Jing, L. Wang, K. Qu, R. Li, W. Kang, H. Li, S. Xiong, KOH Chemical-Activated Porous Carbon Sponges for Monolithic Supercapacitor Electrodes, ACS Appl. Energy Mater. 4 (7) (2021) 6768–6776, https://doi.org/10.1021/acsaem.1c00868.
- [12] F.T. Johra, W.G. Jung, Hydrothermally reduced graphene oxide as a supercapacitor, Appl. Surf. Sci. 357 (2015) 1911–1914, https://doi.org/10.1016/j. apsusc.2015.09.128.
- [13] X. Ke, F. Yang, H. Huang, R. Zhao, J. Huang, J. Ji, L. Li, Stable polyaniline/sodium alginate/graphene oxide composite hydrogels as binder-free supercapacitor electrodes, *Ionics* 28 (12) (2022) 5633–5641.

- [14] L. Li, K. Wang, Z. Huang, C. Zhang, T. Liu, Highly ordered graphene architectures by duplicating melamine sponges as a three-dimensional deformation-tolerant electrode, *Nano Res.* 9 (2016) 2938–2949.
- [15] P. Li, E. Shi, Y. Yang, Y. Shang, Q. Peng, S. Wu, J. Wei, K. Wang, H. Zhu, Q. Yuan, Carbon nanotube-polypyrrole core-shell sponge and its application as highly compressible supercapacitor electrode, *Nano Res.* 7 (2014) 209–218.
- [16] P. Li, Y. Yang, E. Shi, Q. Shen, Y. Shang, S. Wu, J. Wei, K. Wang, H. Zhu, Q. Yuan, Core-double-shell, carbon nanotube@ polypyrrole@ MnO2 sponge as freestanding, compressible supercapacitor electrode, ACS Appl. Mater. Interfaces 6 (7) (2014) 5228–5234.
- [17] X. Liang, K. Nie, X. Ding, L. Dang, J. Sun, F. Shi, H. Xu, R. Jiang, X. He, Z. Liu, Highly compressible carbon sponge supercapacitor electrode with enhanced performance by growing nickel-cobalt sulfide nanosheets, ACS Appl. Mater. Interfaces 10 (12) (2018) 10087–10095.
- [18] H. Liu, T. Xu, Q. Liang, Q. Zhao, D. Zhao, C. Si, Compressible cellulose nanofibrils/ reduced graphene oxide composite carbon aerogel for solid-state supercapacitor, *Adv. Compos. Hybrid Mater.* 5 (2) (2022) 1168–1179.
- [19] N. Liu, Y. Ma, Z. Xu, Y. Guo, X. Luo, High-performance supercapacitor and antifouling biosensor based on conducting polyaniline-hyaluronic acid hydrogels, J. Mater. Sci. 58 (3) (2023) 1171–1182.
- [20] Q. Liu, L. Zang, X. Qiao, J. Qiu, X. Wang, L. Hu, J. Yang, C. Yang, Compressible allin-one supercapacitor with adjustable output voltage based on polypyrrole-coated melamine foam, Adv. Electron. Mater. 5 (12) (2019) 1900724.
- [21] X. Liu, S. Zou, K. Liu, C. Lv, Z. Wu, Y. Yin, T. Liang, Z. Xie, Highly compressible three-dimensional graphene hydrogel for foldable all-solid-state supercapacitor, *J. Power Sources* 384 (2018) 214–222.
- [22] P. Lv, X. Tang, W. Wei, Graphene/MnO 2 aerogel with both high compressiontolerance ability and high capacitance, for compressible all-solid-state supercapacitors, RSC Adv. 7 (74) (2017) 47116–47124.
- [23] R.A. Manzhos, S.A. Baskakov, E.N. Kabachkov, V.I. Korepanov, N.N. Dremova, Y. V. Baskakova, A.G. Krivenko, Y.M. Shulga, G.L. Gutsev, Reduced graphene oxide aerogel inside melamine sponge as an electrocatalyst for the oxygen reduction reaction, *Materials* 14 (2) (2021) 1–12, https://doi.org/10.3390/ma14020322.
- [24] Y. Miao, Y. Xu, C. Hu, J. Liu, Z. Wu, R. Lu, L. Zhang, F. Zhang, Polydopamine/ Melamine Sponge-Derived Compressible Carbon Foam for High-Performance Supercapacitors. *Langmuir* (2025).
- [25] Z. Niu, W. Zhou, X. Chen, J. Chen, S. Xie, Highly compressible and all-solid-state supercapacitors based on nanostructured composite sponge, Adv. Mater. 27 (39) (2015) 6002–6008.
- [26] G. Nyström, A. Marais, E. Karabulut, L. Wågberg, Y. Cui, M.M. Hamedi, Self-assembled three-dimensional and compressible interdigitated thin-film supercapacitors and batteries. *Nat. Commun.* 6 (1) (2015) 7259.
- [27] H. Peçenek, F.K. Dokan, M.S. Onses, E. Yılmaz, E. Sahmetlioglu, Highly compressible binder-free sponge supercapacitor electrode based on flower-like NiO/MnO2/CNT, J. Alloy. Compd. 913 (2022) 165053.
- [28] T. Qian, C. Yu, S. Wu, J. Shen, A facilely prepared polypyrrole–reduced graphene oxide composite with a crumpled surface for high performance supercapacitor electrodes. J. Mater. Chem. A 1 (22) (2013) 6539–6542.
- [29] Y. Ren, Y. Xu, Three-dimensional graphene/metal-organic framework composites for electrochemical energy storage and conversion, *Chem. Commun.* 59 (43) (2023) 6475-6494.
- [30] Y. Shi, G. Liu, R. Jin, H. Xu, Q. Wang, S. Gao, Carbon materials from melamine sponges for supercapacitors and lithium battery electrode materials: A review, *Carbon Energy* 1 (2) (2019) 253–275, https://doi.org/10.1002/cey2.19.
- [31] Y. Song, H. Chen, Z. Su, X. Chen, L. Miao, J. Zhang, X. Cheng, H. Zhang, Highly compressible integrated supercapacitor–piezoresistance-sensor system with CNT–PDMS sponge for health monitoring, Small 13 (39) (2017) 1702091.
- [32] G. Sowmiya, G. Velraj, Designing a ternary composite of PPy-PT/TiO2 using TiO2, and multipart-conducting polymers for supercapacitor application, J. Mater. Sci.

- Mater. Electron. 31 (17) (2020) 14287–14294, https://doi.org/10.1007/s10854-020-03985-5.
- [33] Z.-Y. Sui, Y.-N. Meng, P.-W. Xiao, Z.-Q. Zhao, Z.-X. Wei, B.-H. Han, Nitrogen-doped graphene aerogels as efficient supercapacitor electrodes and gas adsorbents, ACS Appl. Mater. Interfaces 7 (3) (2015) 1431–1438.
- [34] N. Swain, A. Tripathy, A. Thirumurugan, B. Saravanakumar, L. Schmidt-Mende, A. Ramadoss, A brief review on stretchable, compressible, and deformable supercapacitor for smart devices, *Chem. Eng. J.* 446 (P3) (2022) 136876, https://doi.org/10.1016/j.cej.2022.136876.
- [35] X. Tao, S. Ye, K. Zhu, L. Dou, P. Cui, J. Ma, C. Zhao, X. Wei, L. Guo, A. Hojjati-Najafabadi, ATMP doped conductive PANI/CNTs composite hydrogel electrodes toward high energy density flexible supercapacitors, ACS Appl. Energy Mater. 6 (15) (2023) 8177–8188.
- [36] B. Wang, Q. Liu, D. Sun, M. Liu, Y. Lu, X. Liu, L. Yang, Y. Wang, M. Li, D. Wang, Thread electrodes with polypyrrole nanowires for solid state supercapacitors, J. Alloy. Compd. 982 (2024) 173686.
- [37] H. Wang, X. Liu, B. Zhang, J. Yang, Z. Zhang, R. Yue, Z. Wang, Highly compressible supercapacitor based on carbon nanotubes-reinforced sponge electrode, J. Alloy. Compd. 786 (2019) 995–1004.
- [38] W. Wang, J. Jin, Y. Wu, W. Zhang, H. Jiang, X. Li, G. Wang, Unique holey graphene/carbon dots frameworks by microwave-initiated chain reduction for high-performance compressible supercapacitors and reusable oil/water separation, J. Mater. Chem. A 7 (38) (2019) 22054–22062.
- [39] X. Wu, Y. Qiu, W. Cai, J. Li, D. Wu, L. Xu, Y. Kong, Melamine foam supported NiCo2S4/Ag nanowires with charging/discharging induced activation effect for asymmetric supercapacitors, *Chem. Eng. J.* 484 (February) (2024) 149667, https://doi.org/10.1016/j.cej.2024.149667.
- [40] K. Xiao, L.-X. Ding, G. Liu, H. Chen, S. Wang, H. Wang, Freestanding, Hydrophilic Nitrogen-Doped Carbon Foams for Highly Compressible All Solid-State Supercapacitors, Advanced Materials (deerfield Beach, Fla.) 28 (28) (2016) 5907\_6002
- [41] M. Xu, Y. Ma, R. Liu, Y. Liu, Y. Bai, X. Wang, Y. Huang, G. Yuan, Melamine sponge modified by graphene/polypyrrole as highly compressible supercapacitor electrodes, *Synthetic Metals* 267 (June) (2020) 1–9, https://doi.org/10.1016/j. synthmet.2020.116461.
- [42] Z. Yan, S. Luo, Q. Li, Z. Wu, S. Liu, Recent advances in flexible wearable supercapacitors: properties, fabrication, and applications, Adv. Sci. 11 (8) (2024) 2302172.
- [43] J. Yang, X. Ji, L. Liu, Y. Xiang, Y. Zhu, One step fabrication of graphene/ polypyrrole/Ag composite electrode towards compressible supercapacitor, J. Alloy. Compd. 820 (2020) 153081.
- [44] Q. Zhang, X. Gao, X. Liu, J. Mu, Q. Gu, Z. Liu, W. Luo, Flexible wearable energy storage devices: Materials, structures, and applications, *Battery Energy* (2024) 20230061.
- [45] Q. Zhang, X.W. Gao, X. Liu, J.J. Mu, Q. Gu, Z. Liu, W.B. Luo, Flexible wearable energy storage devices: Materials, structures, and applications, *Battery Energy* (2024). https://doi.org/10.1002/bte2.20230061.
- [46] Y. Zhang, A. Xu, Y. Yu, S. Ye, Z. Zhao, W. Cao, S. Zhang, Y. Qin, One-Step Fabrication of Integrated Graphene/Polypyrrole/Carbon Cloth Films for Supercapacitor Electrodes, *Langmuir* 40 (2) (2024) 1399–1407.
- [47] C. Zhao, S. Zhou, J. Ma, C. Liu, J. Zhu, S. Ye, Z. Xin, J. Cai, P. Feng, X. Tao, Highly conductive PANI/ATMP/AgNO 3 composite hydrogel electrodes for all-hydrogelstate supercapacitors, J. Mater. Chem. A (2025).
- [48] X. Zou, H. Liu, Z. Hu, Y. Zhang, J. Cheng, K. Wang, Y. Feng, J. Wang, Rational design of antifreeze and flexible chitosan-based hydrogels for integration device of supercapacitors electrodes and wearable strain sensors, *Carbohydr. Polym.* 123342 (2025).